

Null geodesics, quasinormal modes and the correspondence with shadows in high-dimensional Einstein-Yang-Mills spacetimes

Yang Guo* and Yan-Gang Miao†

School of Physics, Nankai University, Tianjin 300071, China

Null geodesics, quasinormal modes of a massless scalar field perturbation and the correspondence with shadow radii are investigated in the background spacetime of high-dimensional Einstein-Yang-Mills black holes. Based on the properties of null geodesics, we obtain the connection between the radius of a photon sphere and the radius of a horizon in the five- and six-dimensional Einstein-Yang-Mills spacetimes. Especially in the five-dimensional case, there exist two branches for the radius of a photon sphere, but only the branch outside the event horizon satisfies the condition of circular null geodesics. Moreover, we find no reflecting points of shadow radii and no spiral-like shapes on the complex plane of quasinormal frequencies and verify the correspondence between the quasinormal modes in the eikonal limit and shadow radii in high-dimensional Einstein-Yang-Mills spacetimes.

I. Introduction

Quasinormal modes (QNMs) are usually used to depict the stability of black holes that are perturbed by an external field and they also contain the information of gravitational waves. The successful detection of gravitational waves by the LIGO Scientific and Virgo Collaborations [1] opens a new window for the future astronomy, the so-called gravitational wave astronomy. In addition, the images of M87 observed by the Event Horizon Telescope Collaboration [2] show the shadow of the supermassive black hole. The two remarkable achievements mark the beginning of the new era of gravitational wave astronomy, which in turn greatly facilitates the studies of QNMs and shadow radii and their correspondence.

Based on the general relativity and alternative theories of gravity, QNMs have been studied in a wide range of issues [3–8]. Most of the research of QNMs rely on numerical computations, but only a few on analytical computations. For the latter, the lowest QNM frequencies of a vector-type field perturbation have been computed [9] analytically for a generic black hole with a translationally invariant horizon, where the imaginary part of QNM frequencies approaches [10] a large imaginary number plus $\ln 3/(8\pi G_N M)$. Moreover, an analytic computation of highly damped QNMs has been made [11] in term of a monodromy technique.

Now we make a brief review on the correspondence between QNMs and other important issues, such as spacelike geodesics, phase transitions, and null geodesics, etc., which naturally gives our motivation and aim of the present paper. It has been founded [12, 13] that the QNM frequencies in the large black hole mass limit are determined by the spacelike geodesics with the boundary of the Penrose diagram, based on which the quantum aspect of gravity behind horizons can be probed in the context of the gauge/gravity duality. For the four-dimensional Reissner-Nordström (RN) black hole, a spiral-like shape has been shown [14] on the complex plane of QNM frequencies when the black hole evolves to its second order phase transition point. This relation between QNMs and phase transitions gives an opportunity to probe [15] the thermodynamics and dynamics of black holes. Moreover, it has been proposed [16] that the real and imaginary parts of QNMs in the eikonal limit have a compact connection to the angular velocity and Lyapunov exponent of unstable circular null geodesics. Such a correspondence was later extended [17] to investigate the connection between QNMs and the gravitational lensing. However, it has been pointed out [18] for the Einstein-Lovelock theory that the QNM frequencies determined by the angular velocity and Lyapunov exponent deviate from that by the WKB method, which implies that the correspondence between QNMs and null geodesics is violated in the Einstein-Lovelock theory.

Recently, the correspondence between the real part of QNMs in the eikonal limit and shadow radii of black holes has been suggested [19, 20] and applied to a black hole spacetime surrounded by the perfect fluid dark matter, where an interesting discovery is the existence of a reflecting point of shadow radii that corresponds to a maximal value for the real part of QNM frequencies. The connection between QNMs and shadow radii may, alternatively, provide a physical picture at the semi-classical level that the gravitational waves can be understood as such a phenomenon that a massless particle propagates along an outmost and unstable orbit of null geodesics and leaks slowly out to infinity. Based on

*E-mail: guoy@mail.nankai.edu.cn

†Corresponding author E-mail: miaoyg@nankai.edu.cn

the correspondence of Refs. [19, 20] plus a sub-leading contribution derived from the WKB method [21], a modified correspondence between QNMs and shadow radii has been proposed [22] and verified to be a good agreement with the WKB method in the eikonal limit for a D-dimensional Tangherlini black hole and a four-dimensional spherically symmetric black hole surrounded by anisotropic fluids. As stated in our previous work [23], the Einstein-Yang-Mills (EYM) theory [24] is more challenging in finding analytic solutions than the Einstein-Maxwell theory due to the former's intrinsic properties related to QNMs and phase transitions. Therefore, we are interested in whether the modified correspondence between QNMs in the eikonal limit and shadow radii works well or not and also eager for probing the related issues, such as whether a reflecting point of shadow radii and a spiral-like shape on the complex plane of QNM frequencies exist or not in the context of the EYM theory, which aims at our main purpose in this paper. That is, we shall investigate such a correspondence between QNMs in the eikonal limit and shadow radii by dealing with the circular null geodesics of a massless particle around the EYM black holes with the $SO(D-1)$ gauge group.

The outline of the present paper is as follows. In Sec. II we investigate the circular null geodesics of the EYM spacetimes in $D = 5$ and $D = 6$ as an example of $D > 5$ to find the connection between radii of photon spheres and radii of horizons. In order for this paper to be self-contained, we review shortly in Sec. III the derivation of the perturbation equations of a massless scalar field and the calculation of the corresponding QNMs for different values of multiple numbers and overtone numbers by the improved WKB method in a spherically symmetric EYM spacetime. In Sec. IV we focus on the correspondence between the QNMs in the eikonal limit and shadow radii and the related issues. Finally, we give our conclusions in Sec. V. We adopt the geometric unit throughout this paper as usual.

II. Null geodesics

For a D -dimensional static and spherically symmetric spacetime, the metric can be described by

$$ds^2 = -f(r)dt^2 + \frac{dr^2}{f(r)} + r^2d\Omega_{D-2}^2, \quad (1)$$

where $d\Omega_{D-2}^2$ is the line element of the unit sphere S^{D-2} with the usual angular coordinates $\theta_i \in [0, \pi]$, $i = 1, 2, \dots, D-3$, and $\varphi \in [0, 2\pi]$. A freely falling massless particle moving along a null geodesic satisfies the equation,

$$g_{\mu\nu} \frac{dx^\mu}{d\lambda} \frac{dx^\nu}{d\lambda} = 0, \quad (2)$$

where λ is an affine parameter of the null geodesic. In order to give the condition satisfied by circular null geodesics in the above static and spherically symmetric spacetime, Eq. (1), we shall consider a free massless particle orbiting in the equatorial hyperplane ($\theta_i = \pi/2$). Without loss of generality, one has the Lagrangian of a massless particle,

$$\mathcal{L} = \frac{1}{2} \left[-f(r)t^2 + \frac{\dot{r}^2}{f(r)} + r^2\dot{\varphi}^2 \right], \quad (3)$$

where the dot stands for the differentiation with respect to an affine parameter, and there exist two Killing vector fields $\partial/\partial t$ and $\partial/\partial\varphi$ in this spacetime. Correspondingly, one obtains the energy and the angular momentum of the massless particle,

$$E = f(r)\dot{t}, \quad L = r^2\dot{\varphi}. \quad (4)$$

Given these two conserved quantities, one can rewrite the null geodesic equation as follows,

$$\dot{r}^2 = V(r), \quad (5)$$

with the effective potential

$$V(r) = E^2 - \frac{L^2}{r^2}f(r). \quad (6)$$

For a circular null geodesic, the effective potential satisfies [25] the following condition,

$$V(r) = 0, \quad \frac{dV(r)}{dr} = 0, \quad \frac{d^2V(r)}{dr^2} > 0, \quad (7)$$

which can be used to determine the radius of a photon sphere and the instability of the bound circular orbits.

For the five-dimensional Einstein-Yang-Mills black hole, of which the metric is expressed [24] as

$$f(r) = 1 - \frac{M}{r^2} - \frac{2Q^2}{r^2} \ln(r), \quad (8)$$

where M denotes the black hole mass and Q the only non-zero gauge charge, we derive the two branches of the radius of a photon sphere,

$$r_{\text{ps}}^- = \exp \left\{ -\frac{1}{2Q^2} \left[M + Q^2 W_0 \left(-\frac{1}{2Q^2} \exp \left(\frac{Q^2 - 2M}{2Q^2} \right) \right) \right] - Q^2 \right\}, \quad (9)$$

$$r_{\text{ps}}^+ = \exp \left\{ -\frac{1}{2Q^2} \left[M + Q^2 W_{-1} \left(-\frac{1}{2Q^2} \exp \left(\frac{Q^2 - 2M}{2Q^2} \right) \right) \right] - Q^2 \right\}. \quad (10)$$

Here $W_k(x)$, $k = 0, \pm 1, \pm 2, \dots$, are called Lambert's W functions [26], where $W_0(x)$ is referred to as the principal branch. Similarly, for the six-dimensional EYM black hole, of which the metric is expressed [24] as

$$f(r) = 1 - \frac{M}{r^3} - \frac{3Q^2}{r^2}, \quad (11)$$

we have only one radius of a photon sphere,

$$r_{\text{ps}}^+ = \frac{1}{2} \left(10M + 2\sqrt{25M^2 - 128Q^6} \right)^{1/3} + \frac{4Q^2}{\left(10M + 2\sqrt{25M^2 - 128Q^6} \right)^{1/3}}. \quad (12)$$

For the sake of intuition, we plot the radii of photon spheres with respect to the gauge charge Q in Fig. 1 and Fig. 2 in which we can see the connection between the radii of photon spheres and the radii of horizons, where the formulas of the horizon radii can be found in Ref. [24].

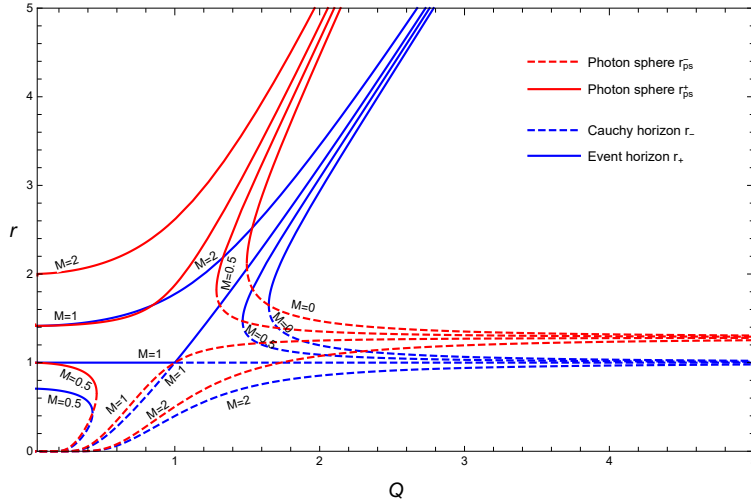


Figure 1: The radii of photon spheres and radii of horizons on the $Q - r$ plane for four different values of black hole masses, $M = 0, 0.5, 1, 2$, in the five-dimensional EYM spacetime.

For the five-dimensional EYM black hole, we can see from Fig. 1 that the position of one branch (red dashed line for r_{ps}^-) of photon sphere radii is located between the Cauchy horizon (blue dashed line for r_-) and the event horizon (blue solid line for r_+), while the position of the other (red solid line for r_{ps}^+) is outside the event horizon. In addition, we find that the branch of photon sphere radii (r_{ps}^-) does not satisfy the first and third points of the condition

Eq. (7). Such properties of photon sphere radii are consistent with the assumption [27] that there exists one photon sphere whose radius satisfies the range of values, $r_{\text{ps}}^+ \in (r_+, \infty)$, which supports the existence of unstable circular null geodesics in the five-dimensional EYM spacetime.

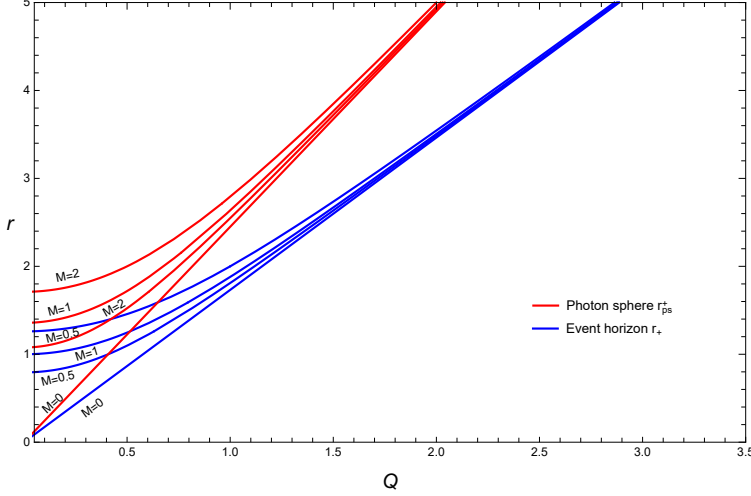


Figure 2: The radii of photon spheres and radii of horizons on the $Q - r$ plane for four different values of black hole masses, $M = 0, 0.5, 1, 2$, in the six-dimensional EYM spacetime.

For the six-dimensional EYM black hole, we can see from Fig. 2 that there is only one photon sphere whose radius (red solid line for r_{ps}^+) is located outside the event horizon (blue solid line for r_+).

As a common property of the five- and six-dimensional EYM spacetimes, it is clear from the two figures that both the radius of a photon sphere and the radius of a horizon are mass independent for a large value of the charge.

III. Quasinormal modes of a massless scalar field perturbation

The massless scalar field Φ propagating in a curved spacetime is described by the following equation,

$$\frac{1}{\sqrt{-g}} \partial_\mu (\sqrt{-g} g^{\mu\nu} \partial_\nu \Phi) = 0, \quad (13)$$

where $g^{\mu\nu}$ denotes the inverse of $g_{\mu\nu}$ and g the determinant of $g_{\mu\nu}$, respectively. Substituting the following decomposition of variables,

$$\Phi(t, r, \Theta, \varphi) = \sum_{l,m} e^{-i\omega t} \frac{\psi(r)}{r^{(D-2)/2}} Y_{lm}(\Theta, \varphi), \quad (14)$$

into Eq. (13), where Θ stands for $\theta_1, \theta_2, \dots, \theta_{D-3}$ and $Y_{lm}(\Theta, \varphi)$ the spherical harmonics of $D-2$ degrees, and defining the “tortoise” coordinate by the relation, $dr_* = dr/f(r)$, we get the following radial equation in its standard form,

$$[\partial_{r_*}^2 + \omega^2 - \mathcal{V}(r)] \psi(r) = 0. \quad (15)$$

The QNMs as the solution of the differential equation satisfy the following boundary conditions,

$$\psi \sim e^{-i\omega(t \mp r_*)}, \quad r_* \rightarrow \pm\infty, \quad (16)$$

and oscillate and decay at a complex frequency, $\omega = \omega_R - i\omega_I$. In the EYM spacetimes, the effective potentials of the perturbation field¹ take [23] the forms,

$$\mathcal{V}(r) = \left(1 - \frac{M}{r^2} - \frac{2Q^2 \ln(r)}{r^2} \right) \left[\frac{4l(l+2)+3}{4r^2} + \frac{9M-12Q^2}{4r^4} + \frac{3Q^2 \ln(r)}{2r^4} \right], \quad D=5, \quad (17)$$

¹The two effective potentials are defined at the semi-classical level, while the effective potential of Eq. (6) has its meaning at the classical level, and the former turns back [28] to the latter in the eikonal limit.

$$\mathcal{V}(r) = \left(1 - \frac{M}{r^{D-3}} - \frac{(D-3)Q^2}{(D-5)r^2}\right) \left[\frac{4l(l+D-3) + (D-2)(D-4)}{4r^2} + \frac{(D-2)^2 M}{4r^{D-1}} - \frac{(D-2)(D-3)(D-8)Q^2}{4(D-5)r^4} \right], \quad D > 5. \quad (18)$$

Now we analyze the behavior of the effective potentials for a changing multiple number l (also called the angular quantum number). We fix the gauge charge Q and the black hole mass M , and then plot Fig. 3 for the effective potentials with respect to the radial coordinate. We find that the effective potentials become large for a big multiple number in both the five- and six-dimensional cases. Moreover, we have calculated the expected QNM frequencies in our previous work [23] by using the improved WKB approximation [29, 30]. As we shall see in the next section, the behaviors of the effective potentials and QNM frequencies for a changing multiple number l will influence the correspondence between QNMs and shadow radii in high-dimensional EYM black holes.

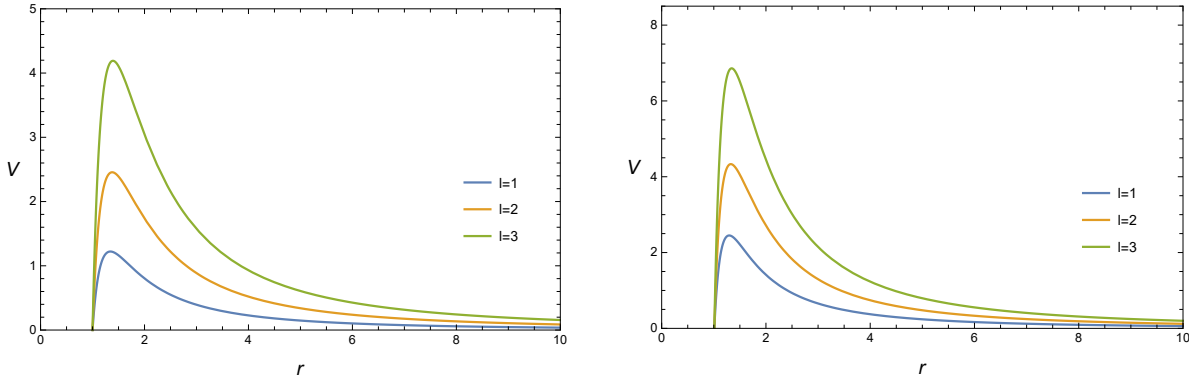


Figure 3: The effective potential with respect to the radial coordinate in the five-dimensional EYM black hole (left) and in the six-dimensional EYM black hole (right) for the fixed charge and mass, $Q = 0.1$ and $M = 1$, but different values of multiple numbers.

IV. Correspondence between QNMs and shadow radii

In general, the shadow shape of a black hole depends on whether the black hole rotates or not. For a static and spherically symmetric black hole, as the EYM black holes we are dealing with, the shadow has the spherical symmetry and is described by the photon sphere. From the definition [31] of a shadow radius, or directly from the concise form [19, 20] expressed in terms of the radius of a photon sphere,

$$R_{\text{sh}} = \frac{r_{\text{ps}}^+}{\sqrt{f(r_{\text{ps}}^+)}}, \quad (19)$$

we obtain the shadow radii in the five- and six-dimensional EYM black holes, respectively, by using Eqs. (8), (10), (11) and (12),

$$R_{\text{sh}} = \frac{\exp\left[-\frac{1}{2Q^2}(M+Q^2\Xi)-Q^2\right]}{\sqrt{1-(M+2Q^2)\left[-\frac{1}{2Q^2}(M+Q^2\Xi)-Q^2\right]\exp\left[\frac{1}{Q^2}(M+Q^2\Xi)+2Q^2\right]}}, \quad D = 5, \quad (20)$$

$$R_{\text{sh}} = \frac{\frac{1}{2}\Re^{1/3} + \frac{4Q^2}{\Re^{1/3}}}{\sqrt{1 - \frac{M}{\left(\frac{1}{2}\Re^{1/3} + \frac{4Q^2}{\Re^{1/3}}\right)^3} - \frac{3Q^2}{\left(\frac{1}{2}\Re^{1/3} + \frac{4Q^2}{\Re^{1/3}}\right)^2}}}, \quad D = 6, \quad (21)$$

where

$$\Xi \equiv W_{-1} \left(-\frac{1}{2Q^2} \exp \left(\frac{Q^2 - 2M}{2Q^2} \right) \right), \quad (22)$$

$$\mathfrak{R} \equiv 10M + 2\sqrt{25M^2 - 128Q^6}. \quad (23)$$

For a spherically symmetric spacetime, the shadows can be plotted [32, 33] more intuitively via the celestial coordinates (α, β) . Here the shadows cast by the five- and six-dimensional EYM black holes are shown in Fig. 4, where the mass parameter is set to be unit, $M = 1$.

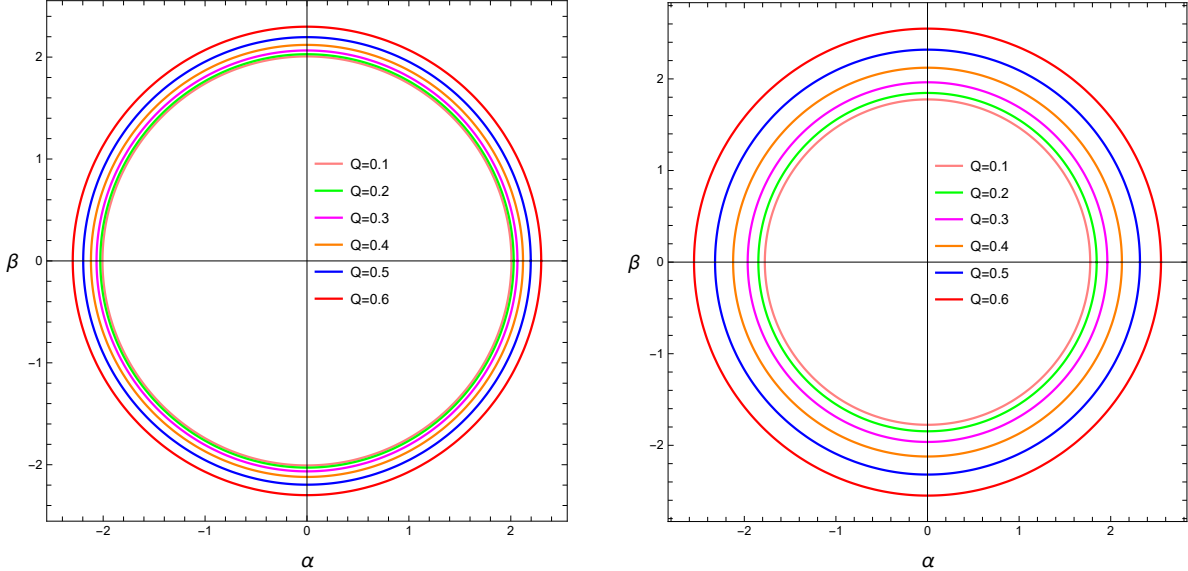


Figure 4: The profile of shadows cast by the five-dimensional EYM black hole (left) and the six-dimensional EYM black hole (right) for six different values of the gauge charge, $Q = 0.1, 0.2, 0.3, 0.4, 0.5, 0.6$.

It is clear from Fig. 4 that the shadow radii increase in the two black holes when the gauge charge increases and that the increments of the shadow radii also increase for an increasing charge but with the same interval, e.g., $\Delta Q = 0.1$. Moreover, the shadow span in the six-dimensional EYM black hole is larger than that in the five-dimensional EYM black hole when the gauge charge is increasing from 0.1 to 0.6. The other property that is worth noting is that there are no reflecting points² at which the shadow radius will shrink with the increasing of the gauge charge.

As revealed by the correspondence between QNMs and null geodesics, the real and imaginary parts of QNM frequencies in the eikonal limit can be determined [16] by the angular velocity Ω and Lyapunov exponent λ ,

$$\omega = \Omega l - i\lambda \left(n + \frac{1}{2} \right), \quad (24)$$

where n is called the overtone number, and the angular velocity and Lyapunov exponent are given by

$$\Omega = \left. \frac{\dot{\phi}}{l} \right|_{r=r_{\text{ps}}^+}, \quad \lambda = \sqrt{\left. \frac{V''(r)}{2l^2} \right|_{r=r_{\text{ps}}^+}}. \quad (25)$$

For the five- and six-dimensional EYM black holes, we calculate the angular velocity and Lyapunov exponent in terms of Eqs. (4), (6), (8), (10), (11) and (12), and then plot in Fig. 5 the angular velocity versus the Lyapunov exponent in a very wide range of values of the gauge charge from 0.0 to 5.0 in order to have a thorough survey.

²The reflecting point exists [19] in the black hole spacetime surrounded by the perfect fluid dark matter, where the metric function contains a logarithmic term. Here we emphasize that no such a reflecting point exists in the five-dimensional EYM black hole although a logarithmic term appears in its metric function, see Eq. (8). This is not strange because the two models have obvious differences from each other. For the former, the reflecting point appears when the dark matter parameter increases; while for the latter, it does not appear when the gauge charge increases.

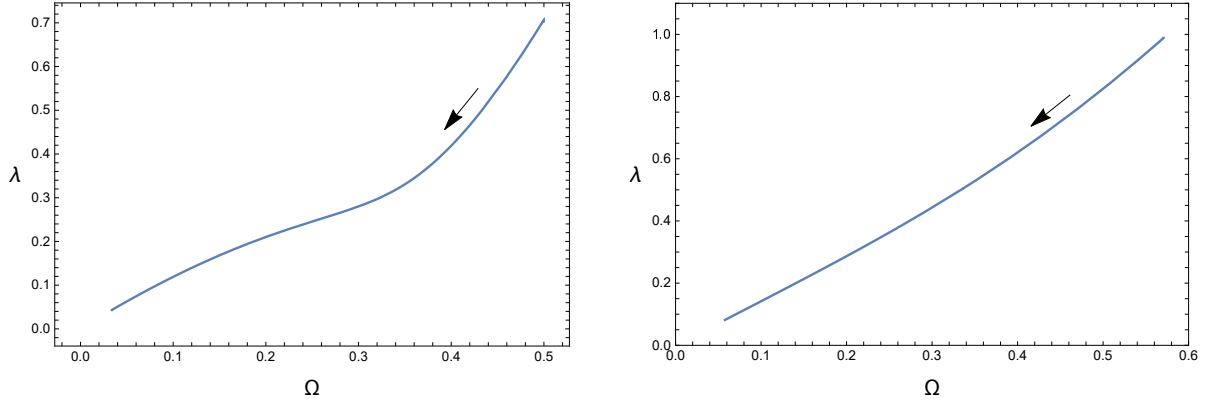


Figure 5: The angular velocity versus the Lyapunov exponent in the five-dimensional EYM black hole (left) and the six-dimensional EYM black hole (right), where the black arrow denotes the direction of the increasing charge.

It is quite obvious that the angular velocity and Lyapunov exponent of the null geodesics are decreasing monotonically with the increasing of the gauge charge from 0.0 to 5.0. Considering the correspondence between QNMs and shadow radii given in Refs. [19, 20], the shadow radius is inversely proportional to the angular velocity in the eikonal limit, we can deduce that the shadow radius does not shrink with the increasing of the gauge charge, that is, no reflecting points appear, which is clear from the monotonic behavior of the angular velocity in Fig. 5. In addition, the monotonic behavior of the Lyapunov exponent indicates that there are no spiral-like shapes³ in high-dimensional EYM black holes, which implies that the high-dimensional EYM black holes have different behaviors of phase transitions from that of the four-dimensional RN black hole because the spiral-like shape on the $\Omega - \lambda$ plane influences [14] thermodynamic phase transitions.

Given the radii of photon spheres, see Eqs. (20)-(23), we can determine the QNM frequencies by the angular velocity and Lyapunov exponent using Eqs. (24) and (25) together with Eqs. (4), (6), (8), (10), (11) and (12). However, we find for the EYM black holes that the real components of frequencies determined by the angular velocity are less than that by the improved WKB approximation for a small multiple number. The reason relies on the fact that the relation between QNMs and null geodesics, Eq. (24), is valid only at a big multiple number, i.e., in the eikonal limit.

In order to overcome the deviation of real parts of QNMs, we appeal to a modified correspondence [22] between QNMs in the eikonal limit and shadow radii of black holes,

$$\omega_R = R_{sh}^{-1} \left(l + \frac{D-3}{2} \right), \quad (26)$$

where the terms of equal and higher orders of l^{-1} have been omitted due to the limit $l \gg 1$. In fact, this modified relation has been derived with the help of the WKB method by adding the sub-leading term $R_{sh}^{-1}(D-3)/2$ to the leading one $R_{sh}^{-1}l$ given by Refs. [19, 20]. Such a correspondence has been verified to coincide with the WKB method at a big multiple number, say, for instance, from 10 to 10^5 , for a D-dimensional Tangherlini black hole and a four-dimensional spherically symmetric black hole surrounded by anisotropic fluids.

Now we turn to investigate the modified relation for high-dimensional EYM black holes, in particular, to the case of a small multiple number. For the five- and six-dimensional EYM black holes, we plot the real part versus the imaginary part of QNM frequencies for different values of the multiple number and the overtone number in Fig. 6. In order to verify the correspondence between the real components of frequencies and the shadow radii, Eq. (26), we compute the QNM frequencies by using Eq. (26) and the imaginary part of Eq. (24) on the one hand, and on the other hand we cite the numerical results we have obtained [23] by using the improved WKB approximation. From Fig. 6, we find that this relation, Eq. (26), is precise enough even if the multiple number is small.⁴ For example, when $l = 2$, $n = 0$, and $Q = 0.5$ are taken for the five-dimensional EYM black hole, the real parts of QNM frequencies

³A recent work has shown [28] that the spiral-like shape exists only in the four-dimensional RN black hole, but does not in high-dimensional RN black holes.

⁴Note that the multiple number was taken to be much bigger than ours in Ref. [22] in order to keep a good agreement with the WKB method for the two models there.

(ω_R) equal 1.366248 and 1.363856 determined by Eq. (26) and the WKB method, respectively. We can see that the deviation of the two numerical values is quite small. As for the six-dimensional model, the corresponding deviation is even smaller. Here we have to make a note that such a consequence is valid only for a vanishing overturn number, $n = 0$, which corresponds to the fundamental mode of QNMs. If the overturn number is bigger than zero, the deviation will be increasing, see Fig. 6 for the case of $n = 1$. For a big multiple number, on the other aspect, Eq. (26) reduces approximately to the real part of Eq. (24), or we can see from Fig. 6 that the real components of frequencies computed by Eq. (26) are very close to the numerical results [23] by the improved WKB approximation. In other words, the bigger the multiple number is, the closer Eq. (26) is to the real part of Eq. (24). As to the imaginary components of QNM frequencies, Fig. 6 shows that the results computed by the imaginary part of Eq. (24) have a very good agreement to that by the improved WKB approximation and further that the smaller the overtone number is, the closer the results from the Lyapunov exponent are to the numerical results from the improved WKB approximation.

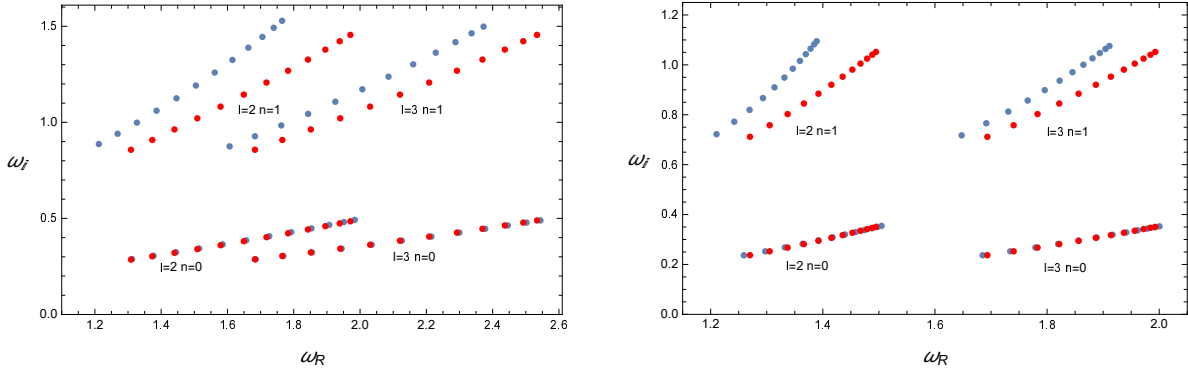


Figure 6: The QNM frequencies on the $\omega_R - \omega_I$ plane for different values of the multiple number and the overtone number. The red dots are given by Eq. (26) and the imaginary part of Eq. (24), and the blue dots by the improved WKB method. The left diagram is devoted to the five-dimensional EYM black hole and the right to the six-dimensional one.

V. Conclusions

We have studied the null geodesics and the correspondence between QNMs in the eikonal limit and shadow radii for high-dimensional EYM black holes. For the five-dimensional case, two branches of the radius of a photon sphere exist, but only the one outside the event horizon satisfies the condition of circular null geodesics. In general, the radii of photon spheres are mass independent when the gauge charge is large, which is same as the behavior of the horizon radii. In addition, the reflecting point of shadow radii and the spiral-like shape on the $\Omega - \lambda$ plane do not appear in high-dimensional EYM spacetimes. In particular, for the modified correspondence between the QNMs in the eikonal limit and shadow radii, Eq. (26), we verify its validity and find that it has a better agreement to the WKB method for a larger multiple number but a smaller overtone number in high-dimensional EYM black holes.

Finally, we emphasize that the modified correspondence, Eq. (26), coincides with the WKB method for the fundamental mode with a vanishing overturn number in high-dimensional Einstein-Yang-Mills spacetimes even if the multiple number is small. The significance of such a consequence is that we establish a deep connection between the modified correspondence and gravitational waves. As is known, the fundamental mode always dominates the waveform of gravitational waves because of its least damped feature in a detected ringdown signal. Although we only discuss the QNMs of a scalar field perturbation in this paper, the QNMs embody the intrinsic property of black holes that are determined by the parameters of black holes, such as mass, charge, etc., and independent of the type of perturbation fields. Our finding might be understood as an exploration of the underlying nature of the correspondence between QNMs and shadows of black holes.

Acknowledgments

This work was supported in part by the National Natural Science Foundation of China under grant No. 11675081.

References

- [1] Ligo Scientic Collaboration and Virgo Collaboration, *Observation of gravitational waves from a binary black hole merger*, Phys. Rev. Lett. **116**, 061102 (2016). [[arXiv:1602.03837 \[gr-qc\]](#)]
- [2] The Event Horizon Telescope Collaboration, *First M87 event horizon telescope results. IV. Imaging the central supermassive black hole*, Astrophys. J. **875**, L4 (2019). [[arXiv:1906.11241 \[astro-ph.GA\]](#)]
- [3] S.H. Hendi and M. Momennia, *Thermodynamic description and quasinormal modes of AdS black holes in Born-Infeld massive gravity with a non-abelian hair*, JHEP **10**, 107 (2019). [[arXiv:1801.07906 \[gr-qc\]](#)]
- [4] R.A. Konoplya, *Quantum corrected black holes: Quasinormal modes, scattering, shadows*, Phys. Lett. **B 804**, 135363 (2020). [[arXiv:1912.10582 \[gr-qc\]](#)]
- [5] R.A. Konoplya, *Analytical representation for metrics of scalarized Einstein-Maxwell black holes and their shadows*, Phys. Rev. **D 100**, 044015 (2019). [[arXiv:1912.10582 \[gr-qc\]](#)]
- [6] S. Yu and C. Gao, *An exact black hole spacetime with scalar field and its shadow together with quasinormal modes*, [arXiv:2001.01137 \[gr-qc\]](#).
- [7] I. Sachs, *Quasi-normal modes for logarithmic conformal field theory*, JHEP **09**, 073 (2008). [[arXiv:0807.1844 \[hep-th\]](#)]
- [8] C. Liu, T. Zhu, Q. Wu, K. Jusufi, M. Jamil, M. Azreg-Aïnou, and A. Wang, *Shadow and quasinormal modes of a rotating loop quantum black hole*, Phys. Rev. **D 101**, 084001 (2020). [[arXiv:2003.00477 \[gr-qc\]](#)]
- [9] A. Starinets, *Quasinormal spectrum and the black hole membrane paradigm*, Phys. Lett. **B 670**, 442 (2009). [[arXiv:0806.3797 \[hep-th\]](#)]
- [10] L. Motl and A. Neitzke, *An analytical computation of asymptotic Schwarzschild quasinormal frequencies*, Adv. Theor. Math. Phys. **6**, 1135 (2003). [[arXiv:gr-qc/0212096](#)]
- [11] L. Motl and A. Neitzke, *Asymptotic black hole quasinormal frequencies*, Adv. Theor. Math. Phys. **7**, 307 (2003). [[arXiv:hep-th/0301173](#)]
- [12] L. Fidkowski, V. Hubeny, M. Kleban, and S. Shenker, *The black hole singularity in AdS/CFT*, JHEP **02**, 014 (2004). [[arXiv:hep-th/0306170](#)]
- [13] G. Festuccia and H. Liu, *Excursions beyond the horizon: Black hole singularities in Yang-Mills theories*, JHEP **04**, 044 (2006). [[arXiv:hep-th/0506202](#)]
- [14] J. Jing and Q. Pan, *Quasinormal modes and second order thermodynamic phase transition for Reissner-Nordström black hole*, Phys. Lett. **B 660**, 13 (2008). [[arXiv:0802.0043 \[gr-qc\]](#)]
- [15] X. He, B. Wang, S. Chen, R.-G. Cai, and C.-Y. Lin, *Quasinormal modes in the background of charged Kaluza-Klein black hole with squashed horizons*, Phys. Lett. **B 665**, 392 (2008). [[arXiv:0802.2449 \[gr-qc\]](#)]
- [16] V. Cardoso, A.S. Miranda, E. Berti, H. Witek, and V.T. Zanchin, *Geodesic stability, Lyapunov exponents, and quasinormal modes*, Phys. Rev. **D 79**, 064016 (2009). [[arXiv:0812.1806 \[hep-th\]](#)]
- [17] I.Z. Stefanov, S.S. Yazadjiev, and G.G. Gylchev, *Null geodesics, quasinormal modes, and thermodynamic phase transition for charged black holes in asymptotically flat and dS spacetimes*, Phys. Rev. Lett. **104**, 251103 (2010). [[arXiv:1003.1609 \[gr-qc\]](#)]
- [18] R.A. Konoplya and Z. Stuchlk, *Are eikonal quasinormal modes linked to the unstable circular null geodesics?*, Phys. Lett. **B 771**, 597 (2017). [[arXiv:1705.05928 \[gr-qc\]](#)]
- [19] K. Jusufi, *Quasinormal modes of black holes surrounded by dark matter and their connection with the shadow radius*, Phys. Rev. **D 101**, 084055 (2020). [[arXiv:1912.13320 \[gr-qc\]](#)]

[20] K. Jusufi, *Connection between the shadow radius and quasinormal modes in rotating spacetimes*, Phys. Rev. **D 101**, 124063 (2020). [[arXiv:2004.04664 \[gr-qc\]](https://arxiv.org/abs/2004.04664)]

[21] S. Iyer and C. M. Will, *Black-hole normal modes: A WKB approach. I. Foundations and application of a higher-order WKB analysis of potential-barrier scattering*, Phys. Rev. **D 35**, 3621 (1987).

[22] B. Cuadros-Melgar, R.D.B. Fontana, and J. de Oliveira, *Analytical correspondence between shadow radius and black hole quasinormal frequencies*, [arXiv:2005.09761 \[gr-qc\]](https://arxiv.org/abs/2005.09761).

[23] Y. Guo and Y.-G. Miao, *Scalar quasinormal modes of black holes in Einstein-Yang-Mills gravity*, [arXiv:2005.07524 \[hep-th\]](https://arxiv.org/abs/2005.07524).

[24] S.H. Mazharimousavi and M. Halilsoy, *Einstein-Yang-Mills black hole solution in higher dimensions by the Wu-Yang ansatz*, Phys. Lett. **B 659**, 471 (2008). [[arXiv:0801.1554 \[gr-qc\]](https://arxiv.org/abs/0801.1554)]

[25] J.M. Bardeen, W.H. Press, and S. A. Teukolsky, *Rotating black holes: Locally nonrotating frames, energy extraction, and scalar synchrotron radiation*, Astrophys. J. **178**, 347 (1972).

[26] R.M. Corless, G.H. Gonnet, D.E.G. Hare, D.J. Jeffrey, and D.E. Knuth, *On the Lambert W function*, Adv. Comput. Math. **5**, 329 (1996).

[27] Y. Decanini, A. Folacci, and B. Raffaelli, *Unstable circular null geodesics of static spherically symmetric black holes, Regge poles, and quasinormal frequencies*, Phys. Rev. **D 81**, 104039 (2010). [[arXiv:1002.0121 \[gr-qc\]](https://arxiv.org/abs/1002.0121)]

[28] S.W. Wei and Y.X. Liu, *Null geodesics, quasinormal modes, and thermodynamic phase transition for charged black holes in asymptotically flat and dS spacetimes*, [arXiv:1909.11911 \[gr-qc\]](https://arxiv.org/abs/1909.11911).

[29] J. Matyjasek and M. Opala, *Quasinormal modes of black holes: The improved semianalytic approach*, Phys. Rev. **D 96**, 024011 (2017). [[arXiv:1704.00361 \[gr-qc\]](https://arxiv.org/abs/1704.00361)]

[30] R.A. Konoplya, A. Zhidenko, and A.F. Zinhailo, *Higher order WKB formula for quasinormal modes and grey-body factors: Recipes for quick and accurate calculations*, Class. Quant. Grav. **36**, 155002 (2019). [[arXiv:1904.10333 \[gr-qc\]](https://arxiv.org/abs/1904.10333)]

[31] V. Perlick, O.Y. Tsupko, and G.S. Bisnovatyi-Kogan, *Influence of a plasma on the shadow of a spherically symmetric black hole*, Phys. Rev. **D 92**, 104031 (2015). [[arXiv:1507.04217 \[gr-qc\]](https://arxiv.org/abs/1507.04217)]

[32] S.E. Vazquez and E.P. Esteban, *Strong field gravitational lensing by a Kerr black hole*, Nuovo. Cim. **B 119**, 489 (2004). [[arXiv:gr-qc/0308023](https://arxiv.org/abs/gr-qc/0308023)]

[33] R. Shaikh, *Black hole shadow in a general rotating spacetime obtained through Newman-Janis algorithm*, Phys. Rev. **D 100**, 024028 (2019). [[arXiv:1904.08322 \[gr-qc\]](https://arxiv.org/abs/1904.08322)]